J Nanopart Res (2015) 17:20
DOI 10.1007/s11051-014-2822-3

RESEARCH PAPER

Role of apoptosis and necrosis in cell death induced by nanoparticle-mediated photothermal therapy

Varun P. Pattani · Jay Shah · Alexandra Atalis · Anirudh Sharma · James W. Tunnell

Received: 21 October 2014 / Accepted: 13 December 2014 / Published online: 13 January 2015

Abstract Current cancer therapies can cause significant collateral damage due to a lack of specificity and sensitivity. Therefore, we explored the cell death pathway response to gold nanorod (GNR)-mediated photothermal therapy as a highly specific cancer therapeutic to understand the role of apoptosis and necrosis during intense localized heating. By developing this, we can optimize photothermal therapy to induce a maximum of 'clean' cell death pathways, namely apoptosis, thereby reducing external damage. GNRs were targeted to several subcellular localizations within colorectal tumor cells in vitro, and the cell death pathways were quantitatively analyzed after photothermal therapy using flow cytometry. In this study, we found that the cell death response to photothermal therapy was dependent on the GNR localization. Furthermore, we demonstrated that nanorods targeted to the perinuclear region irradiated at 37.5 W/cm^2 laser fluence rate led to maximum cell destruction with the 'cleaner' method of apoptosis, at similar percentages as other anti-cancer targeted therapies. We believe that this indicates the therapeutic potential for GNR-mediated photothermal therapy to treat cancer effectively without causing damage to surrounding tissue.

Keywords Gold nanoparticles · Gold nanorods · Photothermal therapy (PTT) · Plasmon resonance · Two-photon imaging · Cancer therapy

V. P. Pattani (✉) · J. Shah · A. Atalis · A. Sharma · J. W. Tunnell
Department of Biomedical Engineering, The University of Texas at Austin, 107 W Dean Keeton, C0800, Austin, TX, USA 78712
e-mail: varun.pattani@utexas.edu

Introduction

Cancer is the second leading cause of death in the USA, in part due to the limitations of the current therapeutics available (Howlader et al. 2012). Approved treatments being used in oncology today include surgery, chemotherapy, and radiation therapy. Both chemotherapy and radiation therapy target all highly proliferating cells within the body affecting not only cancer cells but also causing irreparable harm to the hair follicles, gastrointestinal epithelium, and immune cells. Radiation therapy is relatively localized; however, chemotherapy is systemic and detrimental to the whole body (Frei III E 2000; Mundt et al. 2000; Pollock 2000). As a result, there is demonstrable need for a minimally invasive cancer therapy that 'cleanly' kills cancer cells.

Recently, nanoparticle-mediated photothermal therapy (nPTT) has been explored as an effective method of utilizing heat to treat cancer. nPTT utilizes nanometer-sized exogenous photothermal agents to convert light radiation into thermal energy. Differing

from conventional photothermal therapy or thermal therapy, employing an nPTT agent provides the ability to molecularly target specific biomarkers (e.g., cell surface receptors such as HER2 in specific breast tumors). The ideal nPTT agent is inherently inert, can be targeted to a tumor site, exhibits contrast for imaging, and has high photothermal transduction efficiency. Studies have revealed that gold nanoparticles (GNPs) fulfill those requirements to be effective nPTT agents, as they have been used extensively in vitro and in vivo (Chen et al. 2010a, b; Cole et al. 2009; Dickerson et al. 2008; Huang et al. 2006; Khlebtsov et al. 2006; Khlebtsov and Dykman 2011; Tong et al. 2007).

GNPs are a class of plasmonic nanoparticles, which exhibit localized enhanced surface plasmon resonance (SPR), when fabricated on the nanoscale. The incident electric field induces collective oscillations of surface electrons in resonance with the electric field (El-Sayed 2001; Jain et al. 2006; Khlebtsov et al. 2005). The SPR characteristic frequency depends strongly on the GNP physical and electromagnetic properties. Gold is known to be inert and biocompatible, and toxicity studies have been performed showing GNPs are non-toxic for up to 400 days (Gad et al. 2012). Furthermore, GNPs tend to passively accumulate in cancerous solid epithelial tumor sites due to the enhanced permeability and retention (EPR) effect (Maeda 2001; Maeda et al. 2000). In addition, the gold surface allows for facile bioconjugation of targeting agents through surface modification (Kumar et al. 2008; Liao and Hafner 2005; Liopo et al. 2012).

In this study, we utilized gold nanorods (GNRs), pill-shaped nanoparticles with a high photothermal transduction efficiency (Pattani and Tunnell 2012). Due to their geometry, GNRs have two surface plasmon peaks, with the weaker, untunable peak correlating to the transverse SPR frequency in the visible light range. The second peak, in the near-infrared region (NIR), corresponds to the stronger, longitudinal SPR frequency and is tuned by varying the GNR aspect ratio (length:width) (Brioude et al. 2005; Jain et al. 2006; Lee and El-Sayed 2005). At the peak SPR frequency, GNRs have strong absorption and scattering, which can be exploited for imaging and therapy. The NIR (600–1,000 nm) wavelength range, known as the tissue optical window, is desired for biological applications due to less endogenous scattering and absorption interference (Patterson et al. 1989).

To determine the subcellular GNR localization in vitro, we utilized two-photon microscopy (TPM), which is a laser scanning fluorescence imaging modality that uses a femtosecond tunable laser. TPM generates less out-of-focus signal than either wide-field or confocal microscopy due to spatial confinement of two-photon absorption, allowing for deep imaging and thin optical sectioning resulting in limited photobleaching and three-dimensional reconstruction (Denk et al. 1990; Helmchen and Denk 2002). GNRs strongly absorb the two photons simultaneously in a non-linear process, due to the localized SPR coupling, emitting an extremely strong photoluminescence effect (Durr et al. 2007; Park et al. 2008; Wang et al. 2009), allowing for determining the GNR localization before nPTT.

GNR-mediated nPTT can induce cell death primarily through two pathways: necrosis and apoptosis (Majno and Joris 1995; Trump et al. 1997a). Necrosis is defined as premature injury-related cell death due to external factors, whereas apoptosis is programmed cell death initiated by naturally causing extrinsic and intrinsic factors. During necrosis, cell functions completely break down and the plasma membrane ruptures resulting in the cytoplasmic contents leaking into the extracellular space, leading to inflammation. During the final steps of necrotic cell death, the cells release pro-inflammatory factors from the cytoplasm including alarmin molecules, heat-shock proteins, histones, and cytokines (Szabó 2005; Trump et al. 1997b).

Conversely, apoptosis, a type of programmed cell death, involves a complex signaling pathway induced through intracellular signaling, extracellular receptors, and the mitochondria (Majno and Joris 1995; Trump et al. 1997a). Apoptosis is a standard part of the cell cycle, although it is inhibited in cancer cells to allow for unregulated growth. Typically, it can be instigated by stress from heat, radiation, nutrient deprivation, hypoxia, and viral infection (Green and Reed 1998). Apoptosis is an internal process with little to no extracellular leakage or subsequent inflammation; as a result, this cell death pathway can be considered the 'cleaner' method of killing cells using nPTT.

As a result of the typical heating procedures in nPTT, resulting in high temperatures or microbubble formation, necrosis is most likely the primary cause of cell death during nPTT (Chen et al. 2010a; Tong et al. 2007). Several recent studies have qualitatively suggested that nPTT is dependent on the localization of GNPs and investigated cell death pathways (Huang et al. 2010; Li

and Gu 2010; Tong et al. 2007). Using folate-conjugated GNRs, one group demonstrated that membrane-bound GNRs required a lower energy threshold necessary to induce damage during nPTT than internalized GNRs (Tong et al. 2007). In another study, GNPs in the cytoplasm were presented to be more effective in inducing cell death than GNPs in the nuclei with CW laser irradiation, but the opposite effect was observed for pulsed laser irradiation (Huang et al. 2010). The authors demonstrated, using qualitative assessments by imaging stained cells, that apoptosis and necrosis induction was dependent on GNP localization and laser delivery method, with only necrosis being observed with the pulsed laser irradiation for both localizations. However, another study observed that apoptosis could actually be induced with pulsed laser irradiation and that necrosis had a higher energy threshold to induce damage than the apoptotic threshold (Li and Gu 2010). Due to the dissonance in current literature and the lack of quantitative analysis regarding the cell death response to nPTT, it is necessary to perform a quantitative cell death pathway assessment to truly understand the roles of apoptosis and necrosis during nPTT.

In this study, we aim to show the role of the different cell death pathways, apoptosis and necrosis, which are initiated during nPTT and its dependence on laser parameters and GNR localization. By developing a better understanding of cell death pathway response to GNR localization, we can optimize nPTT to 'cleanly' kill cancer cells, inducing apoptotic cell death mechanisms. GNRs emit localized heating to only the immediate surroundings; therefore, the heating could significantly alter cell death pathways if localized to subcellular locations essential to cell death processes. Due to its limited extracellular damage and lack of inflammatory and immunogenic response, apoptosis is a 'cleaner' cell death pathway than necrosis. As such, we investigated the photothermal parameters, including laser fluence rate and GNR localization, necessary to induce the maximum amount of apoptosis to 'cleanly' kill the cancer cells using nPTT.

Materials and methods

Gold nanorod synthesis

We performed the standard GNR synthesis as previously done by Nikoobakht et al. and Jana et al. in a Ag(I)-assisted growth method (Jana et al. 2001; Nikoobakht and El-Sayed 2003). Briefly, an aqueous gold seed particle solution is prepared by adding 0.01 M $HAuCl_4$ (Sigma Aldrich, St. Louis, MO) to aqueous 0.1 M cetyl tri-methyl-ammonium bromide (CTAB, Sigma Aldrich, St. Louis, MO) solution in a vial, while stirring. Then we made a 0.01 M $NaBH_4$ (CTAB, Sigma Aldrich, St. Louis, MO) solution by placing DI water in a vial, equilibrating it in an ice bath, adding the $NaBH_4$, and mixing it rapidly. The aqueous 0.01 M $NaBH_4$ is added to the gold seed particle solution and stirred for 2 min. Next, an aqueous growth solution is prepared by combining 0.1 M CTAB, 0.01 M $AgNO_3$ (Sigma Aldrich, St. Louis, MO), 0.01 M $HAuCl_4$, and 0.1 M ascorbic acid (Sigma Aldrich, St. Louis, MO). The gold seed solution was then added to this growth solution followed by slowly inverting it two times to mix, which was incubated at 27 °C overnight without stirring. The resulting GNR solution was centrifuged three times at 8,000 RPM for 20 min to remove excess CTAB, to reduce the cytotoxicity, and concentrated in DI H_2O (Alkilany et al. 2009; Wang et al. 2011). We measured the dimensions by averaging over 300 individual particles analyzed in ImageJ (NIH Bethesda, MD) using transmission electron microscopy (TEM, FEI Tecnai, Hillsboro, OR) images. We measured the optical density (OD) using a UV–Vis Spectrophotometer (Beckman Coulter DU720, Brea, CA) and determined the hydrodynamic diameter and surface charge of the GNRs in DI H_2O using a system that combined a dynamic light scatter (DLS) and zeta potential analyzer (ZP) (Zetasizer Nano ZS, Malvern Instruments, Malvern, UK).

Cell culture

Human colorectal tumor cells (HCT-116, ATCC, Manassas, VA) were seeded in T25 flasks with cell culture media composed of McCoy's Modified Medium (Corning CellGro, Corning, NY) supplemented with 10 % fetal bovine serum (FBS) and 1 % penicillin–streptomycin–amphotericin B (Lonza, Basel, Switzerland) at 37 °C with 5 % CO_2. After the cells reached confluence, we detached the cells with 0.5 % trypsin solution (Thermo Scientific HyClone, Waltham, MA) and centrifuged at 600 RPM for 5 min. For TPM imaging, the cells were seeded into 12-well plates with coverslips placed in each well, and

for nPTT cells were seeded into 96-well plates. After reaching ~90 % confluence, we incubated GNRs in fresh culture medium at 0.5 optical density (OD) with the cells.

Two-photon imaging

For TPM imaging, depending on exposure time, we removed the GNR media after 1.5 h and let the cells incubate further in fresh media for varied exposure times to allow for the cellular internalization processes to occur. The cells were allowed to incubate further for 0, 1.5, 4.5, 10.5, and 22.5 h for a total of 1.5, 3, 6, 12, and 24 h post-GNR exposure. After GNR incubation, we removed the media and washed three times with PBS and fixed the cells in 4 % paraformaldehyde (PFA, Fisher Scientific, Waltham, MA) for 10 min. After fixation, we washed with PBS three times and stained the cells with a plasma membrane stain (CellMask, Life Technologies, Carlsbad, CA) for 20 min and washed again with PBS three times. Then we removed the coverslip from the well and mounted it on a glass slide with Vectashield mounting medium (Vector Laboratories, Burlingame, CA) and sealed it with nail polish. Imaging was performed under a TPM (Prairie Technologies, Middleton, WI) with an ultrafast pulsed femtosecond tunable Ti:Sapphire laser (Spectra Physics Mai-Tai, Irvine, CA). The laser was tuned to 800 nm to image the GNRs and 750 nm to image the plasma membrane stain with an incident laser power of ~40 mW. To image the emitted light, we used photomultiplier tubes (PMTs) with a 660 ± 20 nm bandpass filter for the GNRs (Channel 1) and 595 ± 50 nm bandpass filter for the plasma membrane stain (Channel 2). The cells were imaged with a water-immersion 20× objective (Olympus) with a 1.0 NA. All images were taken with the proprietary software (PrairieView) and analyzed with ImageJ (NIH, Bethesda, MD).

Photothermal therapy

To probe cell death pathway initiation after nPTT, we incubated the GNRs in a similar method as for TPM imaging, removing the GNR media after 1.5 h and let the cells incubate further in fresh media for varied exposure times (namely 0, 4.5, and 22.5 h post-GNR incubation) to allow for the cellular internalization processes to occur. Then, we irradiated the cells with an 808 nm CW diode laser (ThorLabs, Newton, NJ), focused to a spot size of 0.15 μm diameter, for 5 min at different fluence rates, ranging from 20 to 50 W/cm^2. During irradiation, we placed the 96-well plates on a heated plate to keep the cells at 37 °C. As a control, we also irradiated cells without GNRs at the highest fluence rate, 50 W/cm^2, without seeing cell death.

Flow cytometry

To analyze the cell death pathways, we stained for apoptosis and necrosis using the Vybrant Apoptosis Assay Kit #4 (Life Technologies, Carlsbad, CA) including YO-PRO-1 (YP, 491/509 nm) and Propidium Iodide (PI, 535/617 nm). The YP dye is a carbocyanine nucleic acid stain that can pervade into apoptotic cells due to the slight membrane permeability, whereas the PI is a DNA-binding stain that is excluded from cells with intact or slightly permeable membranes and will only infuse into the necrotic cells (Idziorek et al. 1995). One hour after nPTT, we washed, trypsinized, centrifuged the cells in microcentrifuge tubes, and then stained the cells with a solution containing YP and PI for 30 min on ice. One study showed that apoptosis and necrosis measurements depend on time after cell injury, in which the authors found that the apoptotic maximum was approximately 1 h after treatment (Lee et al. 2009). As a control, we stained cells with no external effects (negative control), cells exposed to 1 h of UV radiation (apoptotic positive control) and cells exposed to 30 min of lysis buffer (Promega, Madison, WI). To quantitatively measure the YP and PI fluorescence, we used a flow cytometer (BD Accuri C6, Franklin Lakes, NJ) with bandpass filters at 530 nm ± 15 nm (FL1) for YP and >670 nm (FL3) for PI. Cells that are alive have low amounts of YP or PI fluorescence. Apoptotic cells have only moderate YP fluorescence and necrotic cells have high YP and PI fluorescence.

Results

We first characterized the GNRs using TEM to determine the size, UV–Vis to measure the spectra, and DLS and ZP to find the hydrodynamic diameter and surface charge, respectively. Analyzing TEM

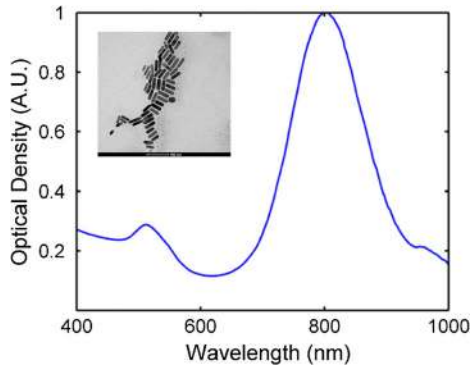

Fig. 1 Absorption spectra for fabricated gold nanorods. *Inset* TEM image of fabricated gold nanorods

images (inset of Fig. 1) with ImageJ (over 300 particles analyzed), we measured the GNR size to be approximately 47 nm in length and 15 nm in width. As shown in the absorbance plot (Fig. 1), the transverse SPR frequency is located $\sim$530 nm, and we tuned the longitudinal peak SPR frequency to a sharp peak $\sim$780 nm, by modifying the aspect ratio to 3.13. With DLS, we observed two hydrodynamic diameter peaks, 3.6 nm with a 37 % contribution and 64.5 nm with a 63 % contribution ($n = 4$), due to the GNR geometry. The GNR zeta potential was observed to be 50.6 mV ($n = 4$) due to the cationic surfactant (CTAB) on the surface.

To determine the GNR localization in vitro, we imaged the cells using TPM after incubation with 0.5 OD GNRs for a range of times: 1.5, 3, 6, 12, and 24 h. We found that the concentration correlated to 0.5 OD was ideal because there was no apparent cytotoxicity within 96 h of incubation yet it was sufficient to induce photothermal damage. TPM can perform thin optical sectioning, which allows us to capture image above the cell, within the cell, and below the cell to accurately define the GNR location. Consequently, we were able to demonstrate that the GNRs were found in varying cellular regions at the different time points as the internalization process advanced (Fig. 2).

In Fig. 2, we display, for each significant time point, a TPM Z-stack imaged through the cells. The Z-stack contains a slice at the top of the cell (1), within the cell (2), and at the bottom of the cell (3). GNRs are observed in the Channel 1 photomultiplier tube (PMT), colored as red, and the cell membrane stain is observed in Channel 2 PMT, colored as green. At the 1.5-h time point, the GNRs appear to be extracellular, accumulating on the cell membrane (Fig. 2). After 3 h of GNR incubation, the GNRs seem to be mainly accumulating on the cell membrane similar to the 1.5-h time point, but with a higher GNR population, based on image intensity. Internalization appears to be more prominent after 6 h (Fig. 2) of incubation with GNRs seemingly aggregating inside the cell. At 12 h (Fig. 2) after incubation, the GNRs appear to be fully internalized in cells and less aggregated. Lastly, at the 24-h time point (Fig. 2), the GNRs seem to accumulate within the cellular perinuclear region. Even though the exact GNR subcellular location at the different time points is vague, it is clear that there is a significant difference in the location for each GNR time point by visually inspecting the images in Fig. 2.

Next, we quantitatively analyzed the cell death pathway response to GNR-mediated nPTT using flow cytometry. We removed the GNRs after 1.5 h of incubation and let the cells incubate the rest of the exposure time (0, 4.5, and 22.5 h post-GNR incubation) to allow for the cellular internalization processes to occur. The extra step of removing GNRs after 1.5 h of incubation was performed to avoid possible influences from final GNR concentration differences in the cell after incubation. We chose these time points because they were significantly different in terms of GNR localization: extracellular GNRs possibly membrane bound (1.5 h), internalized GNRs possibly aggregated in lysosomes (6 h), and internalized GNRs possibly localized to the perinuclear region (24 h).

Flow cytometry was performed on the post-nPTT cell samples to obtain log–log plots (Fig. 3) with the apoptotic stain intensity on the x-axis and the necrotic stain intensity on the y-axis. After gating out the debris, we are left with three distinct regions: (1) the live, (2) apoptotic, and (3) necrotic cells. To determine the three different cell regions, we performed control experiments using solely stained cells (negative control), cells lysed with lysis buffer (necrotic positive control), and cells exposed to 1 h of UV radiation (apoptotic positive control), as shown in Fig. 3a–c, respectively. After determining the regions, we analyzed the cell samples after nPTT and determined the percentage of live, necrotic, and apoptotic cells, as shown in the representative example (6-h-incubated GNRs exposed to 40 W/cm^2) in Fig. 3d. These values were averaged over three replicates for 1.5, 6, and 24-h time points over several fluence rates (35–50 W/cm^2) and compared to each other in bar plots (Fig. 4).

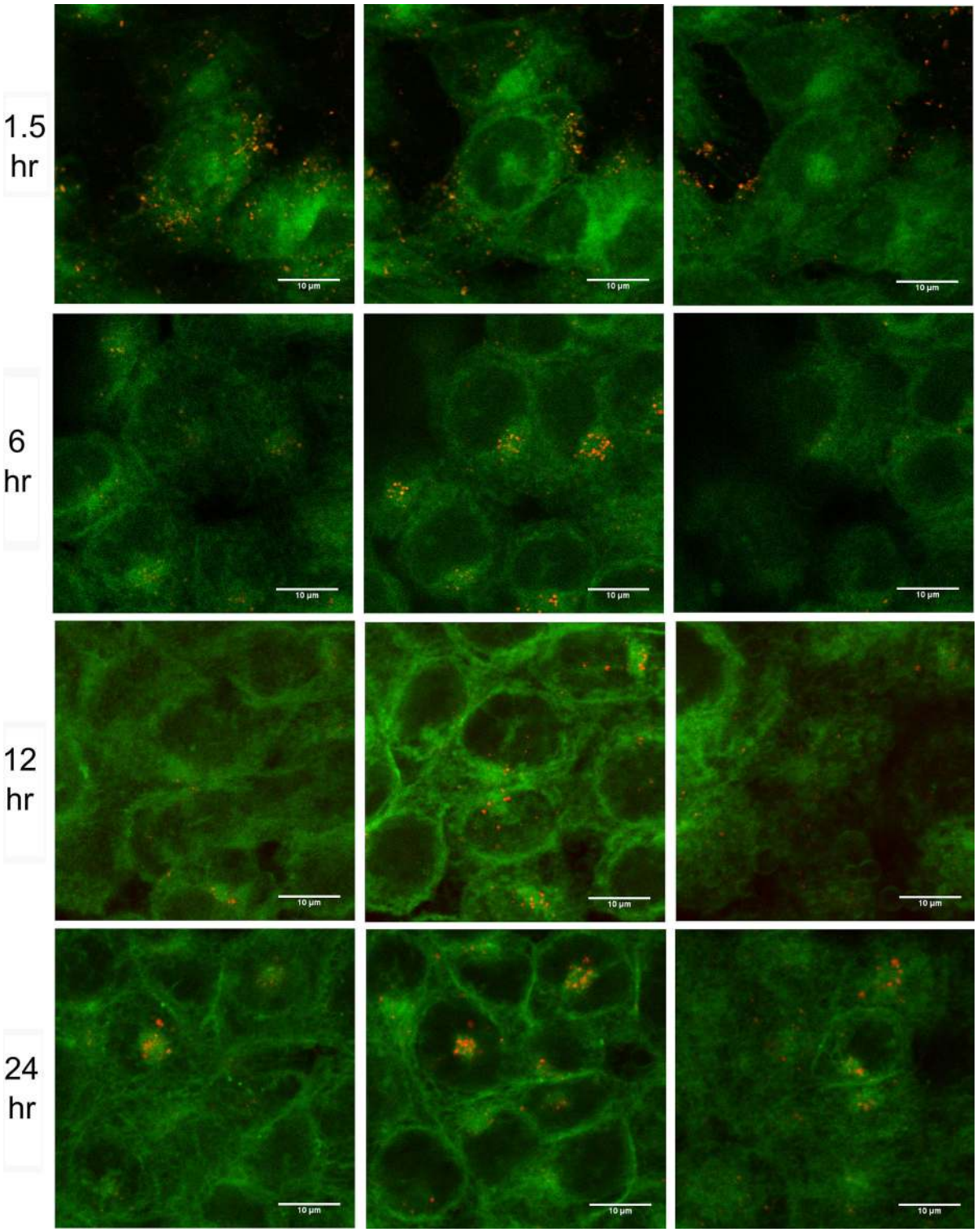
1.5 hr
6 hr
12 hr
24 hr
10 µm

◀**Fig. 2** GNR internalization. All sets show three images through the cell: left is the directly above the cells, middle is ~4 μm below within the cell, right is ~4 μm more to directly below the cell. The 1.5-h-incubated GNRs (*red*) were bound to the top, sides, and bottom of cells (*green*, cell membrane). The 6-h-incubated GNRs were internalized into lysosomes within the cell. The GNRs were escaping from lysosomes into the cytoplasm at 12-h GNR incubation. The final set shows GNRs internalized within the cell and accumulation in the perinuclear area near specific organelles after 24-h GNR incubation. (Color figure online)

From Fig. 4, it is clear to see that the necrotic threshold (~50 %) is the highest for the shortest time point. The necrotic threshold for the 1.5-h time point was 50 W/cm^2, the 6 h was 47.5 W/cm^2, and the 24 h was 42.5 W/cm^2. However, the apoptotic percentage was significantly less than the necrotic percentages. Apoptosis thresholds followed a similar trend as the necrotic thresholds, as the longer incubation times had a lower apoptotic fluence rate threshold. Furthermore, the longer incubation times had higher apoptotic percentages at the threshold, ~18.5 % for 24-h incubation time at 37.5 W/cm^2 (~3× the control), ~13 % for 6-h incubation time at 40 W/cm^2 (~2× the control), and ~9.2 % for 1.5-h incubation time at 42.5 W/cm^2 (~1.5× the control).

Discussion

Using two-photon imaging, we were able to determine the GNR localization at several different time points. Our hypothesis that GNRs would be found in different cellular regions as the cellular internalization process progressed in time was shown to be accurate. We believe this is due to the cationic surfactant, CTAB, bound to the GNR surface. Since the cells are negatively charged and the membrane is composed of lipids, the positive zeta potential and lipophilic

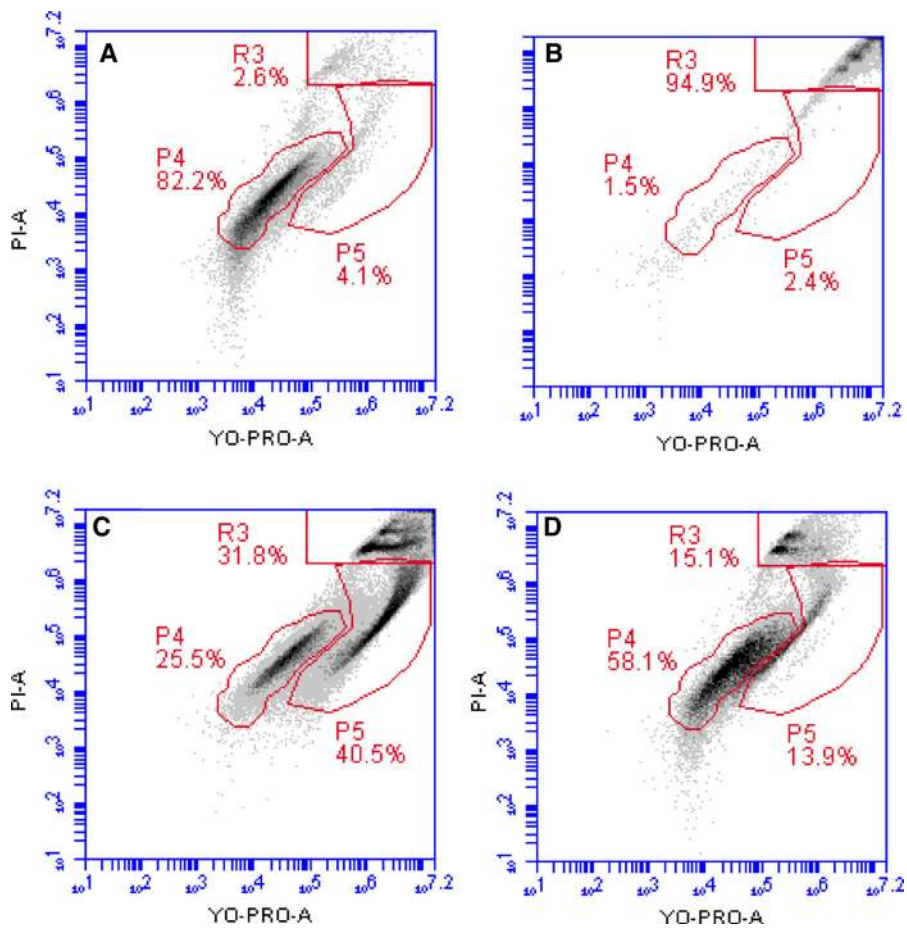

Fig. 3 Flow Cytometry region determination. Log–log plot of fluorescence intensity, apoptosis stain (YP) on the x-axis and necrosis stain (PI) on the y-axis. **a** shows the negative control of only cells stained. **b** shows the necrotic positive control to determine the necrotic region. **c** shows the apoptotic positive control to determine the live, apoptotic, and necrotic regions. **d** Representative sample of cells incubated with GNRs for 6 h and exposed to 40 W/cm^2 irradiation

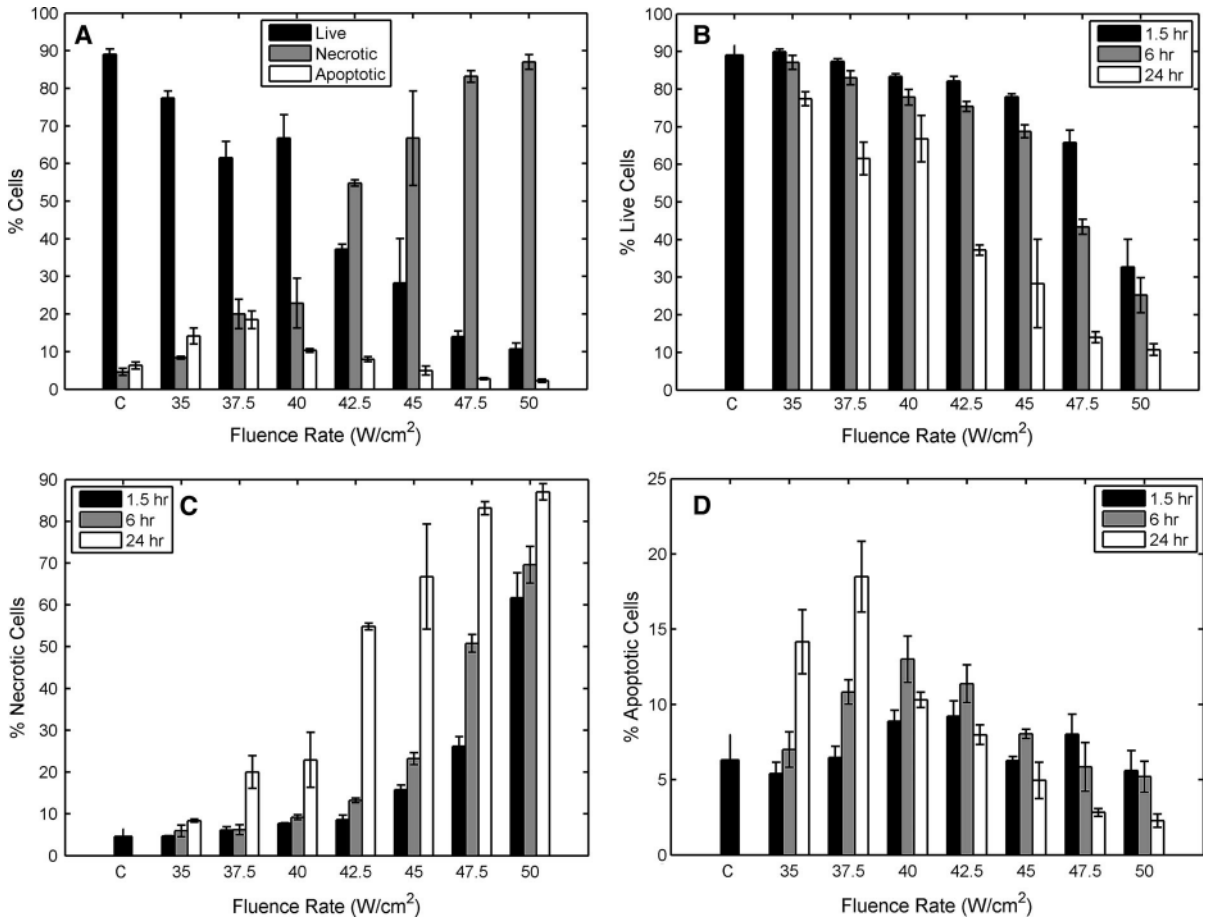

Fig. 4 Quantitative Analysis of Cell Death Response to nPTT. In **a** we see the 24-h-incubated GNRs live, necrotic, and apoptotic percentages for several fluence rates and see the trends. In **b–d** we see the live, necrotic, and apoptotic cell percentages, respectivel,y with all three GNR incubation times compared together at several fluence rates

nature will be attracted to the cellular membrane. This was demonstrated at the 1.5-h time point and continued to the 3-h time point (Fig. 2). The lipophilic cell membrane allows the CTAB GNRs to be transported through the membrane into the cell, possibly into lysosomes, which starts at the 3-h time point, but is more noticeable at the 6-h time point (Fig. 2). The GNRs at the 6-h time point appear to be aggregated and compartmentalized, possibly in lysosomes. After the 6-h time point, we believe that the GNRs escape from the lysosome, and the surface CTAB targets subcellular organelles with lipid membranes, such as the nuclei and mitochondria as shown in previous studies (Tong et al. 2007; Wang et al. 2011). The cell membrane stain that we use is also lipophilic and when internalized also appears to localize to cellular organelles with lipid membranes. At the 24-h time point (Fig. 2), the GNRs appear to be co-localized to the perinuclear region where the cell membrane stain is located within the cell, which we believe to be adjacent to mitochondria or nuclei as other studies have shown (Tong et al. 2007; Wang et al. 2011).

To illustrate an analytical understanding of the cell death pathway response to nPTT, we obtained quantitative values of the number of apoptotic, necrotic, and live cells (Fig. 4). The live cell percentage decreases consistently, for all incubation times, as the fluence rate increases with overall cell death composed of differing ratios of necrosis and apoptosis. Consequently, necrosis increases, for all incubation times, as the fluence rate increases. After the necrotic threshold—defined as the fluence rate when the necrosis percentage is greater than 50 %—necrosis becomes the dominant cell death pathway. As shown

in Fig. 4, the 24-h time point, organelle-localized GNRs, has the lowest necrotic threshold fluence rate and the 1.5-h time point, membrane-bound GNRs, has the highest fluence rate at the threshold. Thus, the internalized GNRs require less energy to induce necrosis suggesting strongly that necrotic initiation depends on GNR localization.

This result is contrary to a study performed by Wei and coworkers; however, we believe that the differences in the experiment, that we use a CW laser and that we have a quantitative measurement of the necrotic cell death, can explain these disparities (Tong et al. 2007). The authors used a pulsed laser in CW mode, which involves a scan of laser pulses over a larger area with approximately 0.126-ms exposure for each nanorod. This is a quasi-CW mode, at the equivalent of millisecond pulses at each point, and could induce photodestructive effects instead of only thermal effects due to the miniscule GNP relaxation time ($\sim$0.6 ns) (Zharov et al. 2005). Secondly, the authors assessed cell death subjectively using qualitative measures such as imaging the ethidium bromide stain and visually inspecting for membrane blebbing, which is representative of both necrosis and apoptosis. Qualitative measures for detecting cell death were also used by El-Sayed and coworkers when demonstrating that cytoplasmic gold nanoparticles required less energy to induce cell death than nuclear localized gold nanoparticles (Huang et al. 2010). We believe the internalized GNR heating profile can induce cell death at lower fluence rates because the thermal energy is localized and spreads evenly throughout the cell to induce cell death through 'cleaner' mechanisms. These mechanisms include mitochondrial or nuclear perturbation, which can induce apoptosis rather than membrane lysis through which cytoplasmic contents leak out and inflammation is induced.

We determined that the apoptotic percentages increased to a maximum value and decreased at or before reaching the necrotic threshold fluence rate, for all samples. This indicates that there is an apoptotic threshold at which apoptosis and necrosis have approximately equal contributions to cell death, which is consistently at a lower fluence rate than the necrotic threshold. When the necrotic threshold is reached, necrosis becomes the dominant cell death pathway leading to decrease in the apoptotic cell death percentage. We observed the maximum apoptotic percentage, thus the maximum of the 'clean' cell death, with the 24-h-incubated GNRs, around 3x the control. This was likely due to the GNR localization to subcellular organelles, which can influence the apoptotic pathway (Wang et al. 2011). One possible pathway of inducing apoptosis involves disrupting the outer mitochondrial membrane, which would release pro-apoptotic effector proteins, such as cytochrome c, initiating the process. The 1.5-h time point had the lowest apoptotic percentage, which we believe is due to the membrane localization where the heating would elicit membrane damage and induce necrosis, suggesting that the apoptotic initiation is affected by GNR localization during nPTT. Another possibility is that the thermal energy was localized to the nuclei, which could inactivate the nucleic acids leading to an induction of the apoptotic pathway.

The apoptotic percentage is shown to be lower than the necrotic percentage; nevertheless, apoptosis is significant when compared to the control, 1.5x for 1.5 h, 2x for 6 h, and 3x for 24-h time points. In cancer, the apoptotic pathway is inhibited such that unregulated proliferation can occur, which may cause resistance to apoptosis in certain cancer types. Previous studies have performed flow cytometry to measure apoptotic percentages with anti-cancer therapeutics, such as doxorubicin, tumor necrosis factor-related apoptosis inducing ligand (TRAIL), CD95, and non-steroidal anti-inflammatory drugs. These studies have observed induced apoptosis percentages for these anti-cancer drugs and therapeutics ranging from 10 to 40 % depending on the therapeutic effectiveness to the specific cell type (Friesen et al. 1996; Fulda et al. 1997; Fulda et al. 2002; Hanif et al. 1996). Therefore in comparison to our study, we see that the 6- and 24-h time points have apoptotic percentages of $\sim$13 and $\sim$18.5 %, respectively, which are in the same range seen for anti-cancer therapeutics. Furthermore, our study has only explored nPTT on colon cancer cells, which can vary for different cell types. We believe that this indicates that for nPTT with specifically localized GNRs, we can achieve a similar anti-cancer therapeutic effect.

Conclusions

Our goal in this study was to quantitatively analyze the role of the cell death response, apoptotic and necrotic, during nPTT to better understand and optimize the therapeutic process for 'clean' cell death killing,

which can be achieved by inducing maximum apoptosis. Therefore, we consider these experimentally determined points to be the optimal parameters for 'clean' GNR-mediated nPTT killing, which should limit the extracellular collateral damage to the surrounding normal tissue. In this study, we investigated the time-dependent GNR internalization process by targeting GNRs to different cell regions based on incubation time. Using TPM, we observed that GNRs were membrane bound at 1.5-h incubation time, starting to be internalized in lysosomal compartments at the 6-h time point, and localized to the perinuclear space, hypothesized to be near organelles, at the 24-h time point. At each time point, we performed nPTT on colon cancer cells incubated with GNRs to quantitatively determine the role of cell death response, specifically apoptosis and necrosis, due to highly localized GNR heating. We found that the 1.5-h time point required the highest fluence rate to induce necrosis and apoptosis, while the 24-h time point required the lowest fluence rate for both. In addition, nPTT at the 24-h time point, which comprised internalized GNRs localized to organelles in the perinuclear space, resulted in the highest apoptotic percentage, ($\sim$18.5 %) while the 6-h time point ($\sim$13 %) and 1.5-h time points (9.2 %) were less. Furthermore, the 24-h and 6-h time points had similar apoptosis values as other anti-cancer therapeutics. In conclusion, we believe these data indicate that the cell death pathway response to nPTT is influenced by GNR localization, which we can utilize to optimize GNR-mediated nPTT to 'cleanly' kill cells by inducing maximum apoptosis.

Acknowledgments We acknowledge the National Institutes of Health (Grant R01CA132032) for the financial support of this work. Additionally, we acknowledge the two-photon microscope use in the project described was supported by Award Number S10RR027950 from the National Center for Research Resources. The content is solely the responsibility of the authors and does not necessarily represent the official views of the National Center for Research Resources or the National Institutes of Health.

Conflict of interest The authors have no conflicts of interest to report.

References

Alkilany AM, Nagaria PK, Hexel CR, Shaw TJ, Murphy CJ, Wyatt MD (2009) Cellular uptake and cytotoxicity of gold nanorods: molecular origin of cytotoxicity and surface effects. Small 5:701–708. doi:10.1002/smll.200801546

Brioude A, Jiang XC, Pileni MP (2005) Optical properties of gold nanorods: DDA simulations supported by experiments. J Phys Chem B 109:13138–13142

Chen CL et al (2010a) In situ real-time investigation of cancer cell photothermolysis mediated by excited gold nanorod surface plasmons. Biomaterials 31:4104–4112. doi:10.1016/j.biomaterials.2010.01.140

Chen H, Shao L, Ming T, Sun Z, Zhao C, Yang B, Wang J (2010b) Understanding the photothermal conversion efficiency of gold nanocrystals. Small 6:2272–2280. doi:10.1002/smll.201001109

Cole JR, Mirin NA, Knight MW, Goodrich GP, Halas NJ (2009) Photothermal efficiencies of nanoshells and nanorods for clinical therapeutic applications. J Phys Chem C 113:12090–12094

Denk W, Strickler JH, Webb WW (1990) Two-photon laser scanning fluorescence microscopy. Science 248:73

Dickerson EB et al (2008) Gold nanorod assisted near-infrared plasmonic photothermal therapy (PPTT) of squamous cell carcinoma in mice. Cancer Lett 269:57–66. doi:10.1016/j.canlet.2008.04.026

Durr NJ, Larson T, Smith DK, Korgel BA, Sokolov K, Ben-Yakar A (2007) Two-photon luminescence imaging of cancer cells using molecularly targeted gold nanorods. Nano Lett 7:941–945. doi:10.1021/nl062962v

El-Sayed MA (2001) Some interesting properties of metals confined in time and nanometer space of different shapes. Acc Chem Res 34:257–264

Frei III E AK (2000) Principles of dose, schedule, and combination chemotherapy. In: al Be (ed) Cancer medicine. BCDecker, Hamilton

Friesen C, Herr I, Krammer PH, Debatin K-M (1996) Involvement of the CD95 (APO–1/Fas) receptor/ligand system in drug–induced apoptosis in leukemia cells. Nat Med 2:574–577

Fulda S, Sieverts H, Friesen C, Herr I, Debatin K-M (1997) The CD95 (APO-1/Fas) system mediates drug-induced apoptosis in neuroblastoma cells. Cancer Res 57:3823–3829

Fulda S, Wick W, Weller M, Debatin K-M (2002) Smac agonists sensitize for Apo2L/TRAIL-or anticancer drug-induced apoptosis and induce regression of malignant glioma in vivo. Nat Med 8:808–815

Gad SC, Sharp KL, Montgomery C, Payne JD, Goodrich GP (2012) Evaluation of the toxicity of intravenous delivery of auroshell particles (gold-silica nanoshells). Int J Toxicol 31:584–594. doi:10.1177/1091581812465969

Green DR, Reed JC (1998) Mitochondria and apoptosis. Science 281:1309–1312

Hanif R et al (1996) Effects of nonsteroidal anti-inflammatory drugs on proliferation and on induction of apoptosis in colon cancer cells by a prostaglandin-independent pathway. Biochem Pharmacol 52:237–245

Helmchen F, Denk W (2002) Deep tissue two-photon microscopy. Nature 12(5):593–601

Howlader N et al (2012) SEER cancer statistics review, 1975–2009 (vintage 2009 populations). National Cancer Institute, Bethesda

Huang XH, El-Sayed IH, Qian W, El-Sayed MA (2006) Cancer cell imaging and photothermal therapy in the near-infrared

region by using gold nanorods. J Am Chem Soc 128:2115–2120. doi:10.1021/ja057254a

Huang X et al (2010) Comparative study of photothermolysis of cancer cells with nuclear-targeted or cytoplasm-targeted gold nanospheres: continuous wave or pulsed lasers. J Biomed Optics 15:058002. doi:10.1117/1.3486538

Idziorek T, Estaquier J, De Bels F, Ameisen J-C (1995) YO-PRO-1 permits cytofluorometric analysis of programmed cell death (apoptosis) without interfering with cell viability. J Immunol Methods 185:249–258

Jain PK, Lee KS, El-Sayed IH, El-Sayed MA (2006) Calculated absorption and scattering properties of gold nanoparticles of different size, shape, and composition: Applications in biological imaging and biomedicine. J Phys Chem B 110:7238–7248. doi:10.1021/jp057170o

Jana NR, Gearheart L, Murphy CJ (2001) Wet chemical synthesis of high aspect ratio cylindrical gold nanorods. J Phys Chem B 105:4065–4067

Khlebtsov N, Dykman L (2011) Biodistribution and toxicity of engineered gold nanoparticles: a review of in vitro and in vivo studies. Chem Soc Rev 40:1647–1671

Khlebtsov N, Trachuk L, Mel'nikov A (2005) The effect of the size, shape, and structure of metal nanoparticles on the dependence of their optical properties on the refractive index of a disperse medium. Opt Spectrosc 98:77–83

Khlebtsov B, Zharov V, Melnikov A, Tuchin V, Khlebtsov N (2006) Optical amplification of photothermal therapy with gold nanoparticles and nanoclusters. Nanotechnology 17:5167

Kumar S, Aaron J, Sokolov K (2008) Directional conjugation of antibodies to nanoparticles for synthesis of multiplexed optical contrast agents with both delivery and targeting moieties. Nat Protoc 3:314–320. doi:10.1038/nprot.2008.1

Lee KS, El-Sayed MA (2005) Dependence of the enhanced optical scattering efficiency relative to that of absorption for gold metal nanorods on aspect ratio, size, end-cap shape, and medium refractive index. J Phys Chem B 109:20331–20338. doi:10.1021/jp054385p

Lee J, Lilly GD, Doty RC, Podsiadlo P, Kotov NA (2009) In vitro toxicity testing of nanoparticles in 3D cell culture. Small 5:1213–1221. doi:10.1002/smll.200801788

Li JL, Gu M (2010) Surface plasmonic gold nanorods for enhanced two-photon microscopic imaging and apoptosis induction of cancer cells. Biomaterials 31:9492–9498. doi:10.1016/j.biomaterials.2010.08.068

Liao HW, Hafner JH (2005) Gold nanorod bioconjugates. Chem Mater 17:4636–4641. doi:10.1021/cm050935k

Liopo A, Conjusteau A, Tsyboulski D, Ermolinsky B, Kazansky A, Oraevsky A (2012) Biocompatible gold nanorod conjugates for preclinical biomedical research. J Nanomed Nanotechnol. doi:10.4172/2157-7439.S2-001

Maeda H (2001) The enhanced permeability and retention (EPR) effect in tumor vasculature: The key role of tumor-selective macromolecular drug targeting. Adv Enzyme Regul 41:189–207

Maeda H, Wu J, Sawa T, Matsumura Y, Hori K (2000) Tumor vascular permeability and the EPR effect in macromolecular therapeutics: a review. J Controlled Release 65:271–284

Majno G, Joris I (1995) Apoptosis, oncosis, and necrosis. An overview of cell death. Am J Pathol 146:3

Mundt A, Roeske J, Weichselbaum R (2000) Physical and biologic basis of radiation oncology. In: al Be (ed) Cancer medicine. BCDecker, Hamilton

Nikoobakht B, El-Sayed MA (2003) Preparation and growth mechanism of gold nanorods (NRs) using seed-mediated growth method. Chem Mater 15:1957–1962

Park J et al (2008) Two-photon-induced photoluminescence imaging of tumors using near-infrared excited gold nanoshells. Opt Express 16:1590–1599

Pattani VP, Tunnell JW (2012) Nanoparticle-mediated photothermal therapy: A comparative study of heating for different particle types. Lasers Surg Med 44:675–684

Patterson MS, Chance B, Wilson BC (1989) Time resolved reflectance and transmittance for the non-invasive measurement of tissue optical properties. Appl Opt 28:2331–2336

Pollock R (2000) Principles of Surgical Oncology. In: al Be (ed) Cancer Medicine. BCDecker, Hamilton

Szabó C (2005) Mechanisms of cell necrosis Critical care medicine 33:S530–S534

Tong L, Zhao Y, Huff TB, Hansen MN, Wei A, Cheng JX (2007) Gold nanorods mediate tumor cell death by compromising membrane integrity. Adv Mater 19:3136. doi:10.1002/adma.200701974

Trump BE, Berezesky IK, Chang SH, Phelps PC (1997a) The pathways of cell death: oncosis, apoptosis, and necrosis. Toxicol Pathol 25:82

Trump BE, Berezesky IK, Chang SH, Phelps PC (1997b) The Pathways of Cell Death: Oncosis. Apoptosis, and Necrosis Toxicologic Pathology 25:82–88. doi:10.1177/019262339702500116

Wang DS, Hsu FY, Lin CW (2009) Surface plasmon effects on two photon luminescence of gold nanorods. Opt Express 17:11350–11359

Wang L et al (2011) Selective targeting of gold nanorods at the mitochondria of cancer cells: implications for cancer therapy. Nano Lett 11:772–780. doi:10.1021/nl103992v

Zharov VP, Galitovskaya EN, Johnson C, Kelly T (2005) Synergistic enhancement of selective nanophotothermolysis with gold nanoclusters: Potential for cancer therapy. Lasers Surg Med 37:219–226. doi:10.1002/lsm.20223